EPJ Appl. Metamat. **9**, 14 (2022)

https://doi.org/10.1051/epjam/2022006

EPJ Applied Metamaterials

Available online at:
epjam.edp-open.org

Metamaterials for Novel Wave Phenomena in Microwaves, Optics, and Mechanics

RESEARCH ARTICLE OPEN ACCESS

How to achieve exceptional points in coupled resonators using a gyrator or PT-symmetry, and in a time-modulated single resonator: high sensitivity to perturbations★

Alireza Nikzamir[1], Kasra Rouhi[1], Alexander Figotin[2], and Filippo Capolino[1,*]

[1]Department of Electrical Engineering and Computer Science, University of California, Irvine, CA 92697, USA
[2]Department of Mathematics, University of California, Irvine, CA 92697, USA

Received: 6 December 2021 / Accepted: 25 February 2022

Abstract. We study the rise of exceptional points of degeneracy (EPD) in various distinct circuit configurations such as gyrator-based coupled resonators, coupled resonators with PT-symmetry, and in a single resonator with a time-varying component. In particular, we analyze their high sensitivity to changes in resistance, capacitance, and inductance and show the high sensitivity of the resonance frequency to perturbations. We also investigate stability and instability conditions for these configurations; for example, the effect of losses in the gyrator-based circuit leads to instability, and it may break the symmetry in the PT-symmetry-based circuit, also resulting in instabilities. Instability in the PT-symmetry circuit is also generated by breaking PT-symmetry when one element (e.g., a capacitor) is perturbed due to sensing. We have turned this instability "inconvenience" to an advantage, and we investigate the effect of nonlinear gain in the PT-symmetry coupled-resonator circuit and how this leads to an oscillator with oscillation frequency very sensitive to perturbation. The circuits studied in this paper have the potential to lead the way for a more efficient generation of high-sensitivity sensors that can detect very small changes in chemical, biological, or physical quantities.

Keywords: Coupled resonators / exceptional points of degeneracy (EPDs) / gyrator / perturbation theory / sensor / time-modulation

1 Introduction

In order to improve the detection limit for small perturbation sensors, an operation based on the exceptional point of degeneracy concept (EPD) can be a valuable option. EPD is a point at which two or more eigenvalues and the corresponding eigenvectors of the system coalesce (i.e., they are degenerate) [1–16]. The main feature of an exceptional point is the strong full degeneracy of the relevant eigenmodes (including their eigenvectors), justifying the presence of "D" in EPD that stands for "degeneracy" [17]. Exceptional points have been observed in various circuits as in coupled resonators [18–24], temporally-periodic systems [25–27], and spatially periodic structures [28–30].

Sensors are used widely and extensively in many industrial, automotive, and medical applications. In recent years, numerous approaches have been used to sense variations of physical, biological, or chemical changes, e.g., to sense pressure [18,31,32], temperature [33], humidity [34], electron beam velocity [35], and chemical or biological quantities [36–39]. Since sensitivity is an essential feature of measurement systems, various types of sensors are needed to sense. Thus, low-cost, simple, and highly-sensitive sensors are desirable to measure different quantities. In conventional sensors, the perturbation by a small value Δ results in shifting the system's eigenfrequency by an amount in the same order of Δ (linear behavior), like perturbing a simple LC resonator (or tank). It means that in conventional sensing applications, the perturbation and the measurable changes, like frequency, follow the same trend. To increase the sensitivity, EPDs have offered a new method. Rather than typical detecting systems, where the eigenfrequency changes are of the same order of the perturbation Δ, the change of an eigenfrequency $\Delta\omega$ in a system working at an EPD of order two follows the behavior $\Delta\omega \propto \Delta^{1/2}$ as shown in [40–43]. EPDs are found in many physical settings under PT-symmetry properties [7,18–22,44]. However, EPDs are also found in more general forms, which do not require a system to satisfy PT-symmetry [25–27,40,45]. Breaking

★ Invited article.
* e-mail: f.capolino@uci.edu

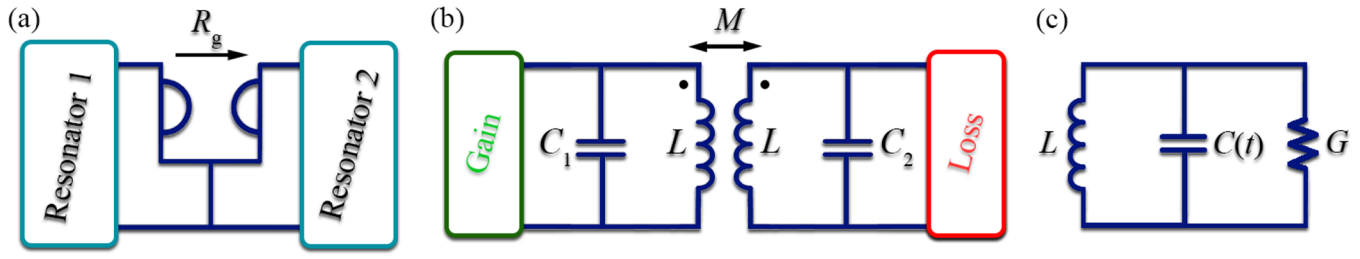

Fig. 1. Three different configurations where support EPD. (a) Two resonators coupled through gyrator. (b) Two mutually coupled-resonator terminated with balanced gain and loss (PT-symmetry circuit). (c) Time-varying circuit which just one component in the circuit needed to change over time periodically. The time-varying component here could be capacitor or inductor or loss.

the symmetry due to the external perturbance eigenvalues split from the degenerated value can be used as a detecting system.

This paper treats EPDs using four methods: First, by using the circuit's characteristic equation and showing the degeneracy of the eigenmodes. Second, the coalescence of eigenvectors, which is observed analytically. Third, time-domain results obtained from simulations show the linear growth revealing the second-order EPD. The related frequency response is also studied, and it is shown how it is associated with the EPD. Fourth, the approximate fractional power expansion series using the Puiseux series shows the bifurcation and square root-like behavior of the eigenvalues with respect to perturbations.

To address the effectiveness of the discussed EPD circuits, we consider the systems' sensitivity to perturbations of capacitance, inductance, and resistance, which are used as sensing elements, depending on the application. In Section 2, we provide an overview of the three circuit configurations leading to second-order EPDs. In Section 3, we describe the second-order EPD in the gyrator-based circuit with parallel configuration in lossless and lossy cases. Also, we study the stability of the circuit, manifested in its eigenfrequencies. Details and analysis of the series configuration, not shown here, are discussed in [23,24,46,47]. In Section 4, we study the second-order EPD in two coupled resonators with balanced gain and loss satisfying PT-symmetry. In this circuit, we consider nonlinear gain, and by perturbing only one side of the coupled resonator, we break PT-symmetry making the system unstable and causing oscillation. In [18], when a perturbation occurs on one side of the coupled resonator circuit, the other side is tuned accordingly to keep PT-symmetry. This procedure made the operational regime difficult to implement since the exact value of the changes should be known a priori. Moreover, the sign of the perturbation was consistent with the bifurcation direction, which means that only either positive or negative changes in the circuit's quantities could be sensed, not both. Instead, working as in the oscillator regime enables sensing of perturbations with both positive and negative signs. Also, when using nonlinear gain and the oscillatory regime, there is no need to tune a circuit's side to keep symmetry, as we show in Section 4. Nonlinearity plays a critical role in this circuit operational regime and helps us find the EPD more easily. While the circuit with EPD and nonlinearity is sensitive to any perturbation sign, the nonlinearity keeps the circuit at an EPD even with a 1% miss-match between the gain and loss. Finally, in Section 5, we study a single LC resonator with a time-varying element and show how this simple configuration leads to an EPD by just tuning the modulation frequency. In order to find the EPD, we assume a time-varying capacitor connected to a fixed inductance. Then, the loss effect is taken into account in the analysis. We study the eigenfrequency dispersion by varying modulation frequency, where the LC tank is connected to loss or gain. Also, EPD is found in the time-modulated circuit when the LC tank is terminated with time-varying gain or loss.

2 Second-order EPD in three distinct possible configurations

We discuss here three different methods to obtain a second-order EPD. First, the degeneracy of the eigenvalues (i.e., eigenfrequencies) occurs in a gyrator-based circuit where two LC tanks are coupled with a gyrator, as shown in Figure 1a. Second, we study two mutually coupled LC circuits with balanced gain and loss, satisfying PT-symmetry, shown in Figure 1b.

In Figures 1a and 1b, both circuits support square root sensitive behavior to perturbations of the resistance, capacitance, and inductance. However, some differences must be observed: for example, the conventional PT-symmetry circuit in Figure 1b needs the tuning on both sides to keep the PT-symmetry and avoid self-oscillations (arising from non-zero Im (ω)). In other words, it is not possible to change one side only and observe two purely real eigenfrequencies. Instead, the gyrator-based circuit shows that the perturbation on only one side leads to two purely real eigenfrequencies. Thus, there is no need to tune the other side after a perturbation in the gyrator-based circuit. However, any gain or loss in the gyrator-based circuit will cause oscillation and instability, as we will discuss later in more detail.

We show how to turn the instability of a circuit (e.g., the one in Figure 1b) to our advantage. Using nonlinear

gain, we make the circuit oscillate and saturate, and by perturbing the capacitance on one side, a square root-like change in oscillation frequency is detected. Working in an oscillator regime has certain advantages compared to the conventional PT-symmetry regime of operations in the previous literature [18]. For instance, there is no need to tune the circuit to reach PT-symmetry again after the perturbed values (of a capacitor, for example) are measured in this circuit. Also, nonlinearity helps to fine-tune the circuit to the EPD in an easier way. We discuss these concepts in more detail later on in Section 4.

The third circuit we discuss here, shown in Figure 1c, is a linear time-varying (LTV) system in which an inductor is connected to the time-varying capacitor. This configuration does not need any negative components to realize the EPD, like a negative capacitance and inductance in the gyrator-based circuit or an active gain element in the PT-symmetric coupled-resonator circuit. In addition, we need only one time-varying resonator in this third scheme rather than two fixed resonators. Similarly, an EPD is found in the LTV circuit when an inductor and capacitor are connected in parallel to the time-varying loss or gain.

3 EPD in gyrator-based circuit

In this section, we study the first scheme to obtain EPD by using two coupled LC tanks connected through a gyrator. An ideal gyrator is a nonreciprocal linear two-port device whose current on one port is related to the voltage on the other port. More details about the gyrator and various realization methods are discussed in references [48–51]. The instantaneous relations between voltages and currents on the gyrator are described by

$$\begin{cases} v_2(t) = R_g i_1(t) \\ v_1(t) = -R_g i_2(t) \end{cases} \tag{1}$$

where the gyration resistance R_g has a unit of Ohm with the direction indicated by an arrow in the circuit.

We find the eigenvalues (i.e., the eigenfrequencies) and demonstrate the condition for obtaining an EPD at the desired frequency. Finally, we show the sensing potentials by applying a perturbation, and we study the effects of losses on the stability of eigenfrequencies. In addition, by using a time-domain circuit simulator, we verify the circuit behavior predicted by the theoretical calculations and also show that the eigenfrequencies can be predicted by using the Puiseux fractional power series expansion.

3.1 Lossless configuration

Two parallel LC tanks are coupled by a gyrator, as shown in Figure 2a. By writing the circuit equations and defining the state vector as $\mathbf{\Psi} \equiv \left[Q_1, Q_2, \dot{Q}_1, \dot{Q}_2\right]^{\mathrm{T}}$, leads to

$$\frac{\mathrm{d}\mathbf{\Psi}}{\mathrm{d}t} = \underline{\mathbf{M}}\mathbf{\Psi}, \tag{2}$$

where

$$\underline{\mathbf{M}} = \begin{bmatrix} 0 & 0 & 1 & 0 \\ 0 & 0 & 0 & 1 \\ -\omega_{01}^2 & 0 & 0 & \dfrac{1}{R_g C_2} \\ 0 & -\omega_{02}^2 & -\dfrac{1}{R_g C_1} & 0 \end{bmatrix} \tag{3}$$

and $\underline{\mathbf{M}}$ is the circuit matrix. The eigenfrequencies of this circuit are calculated by solving the characteristic equation [24,52],

$$\omega^4 - \omega^2\left(\omega_{01}^2 + \omega_{02}^2 + \frac{1}{C_1 C_2 R_g^2}\right) + \omega_{01}^2\omega_{02}^2 = 0. \tag{4}$$

The characteristic equation is quadratic in ω^2 and all the coefficients are real, so both ω and $-\omega$ and ω and ω^* are solutions. The angular eigenfrequencies are determined as

$$\omega_{1,3} = \pm\sqrt{a+b}, \omega_{2,4} = \pm\sqrt{a-b}, \tag{5}$$

$$a = \frac{1}{2}\left(\omega_{01}^2 + \omega_{02}^2 + \frac{1}{C_1 C_2 R_g^2}\right), \tag{6}$$

$$b^2 = a^2 - \omega_{01}^2\omega_{02}^2. \tag{7}$$

According to equation (5), a necessary condition for an EPD to occur is $b = 0$, which results in an EPD angular frequency of $\omega_e = \sqrt{a} = \sqrt{\omega_{01}\omega_{02}}$. So, we rewrite equation (7) as

$$(\omega_{01} - \omega_{02})^2 = -\frac{1}{C_1 C_2 R_g^2}. \tag{8}$$

In order to obtain an EPD with real angular frequency, we consider the case with purely real value for ω_{01} and ω_{02}, so the value of either C_1 or C_2 should be negative. As a result, to have a real value for ω_{01} and ω_{02}, one resonator needs to be composed of both negative C and L, and more details are discussed in [46,47]. Another scenario with an unstable uncoupled resonator is conceivable, which was studied for a series configuration in [23]. As an example, here we use the following values for the components shown in Figure 2a: $L_1 = 100\,\mu\mathrm{H}$, $L_2 = -100\,\mu\mathrm{H}$, $C_2 = -100\,\mathrm{nF}$, and $R_g = 50\,\Omega$. Then, the positive capacitance C_1 is found by solving the quadratic equation obtained from the EPD condition. Since the equation of the EPD condition is quadratic, it would yield two answers for C_1. In this paper, we select the value that leads to real EPD frequency, which is $C_1 = 13.51\,\mathrm{nF}$. Then the corresponding value for EPD angular frequency is calculated as $\omega_e = 5.22 \times 10^5$ rad/s. In this circuit, an opamp-based invertor could realize the negative components. The designed circuit to obtain negative impedance is shown in Figure 2b, which

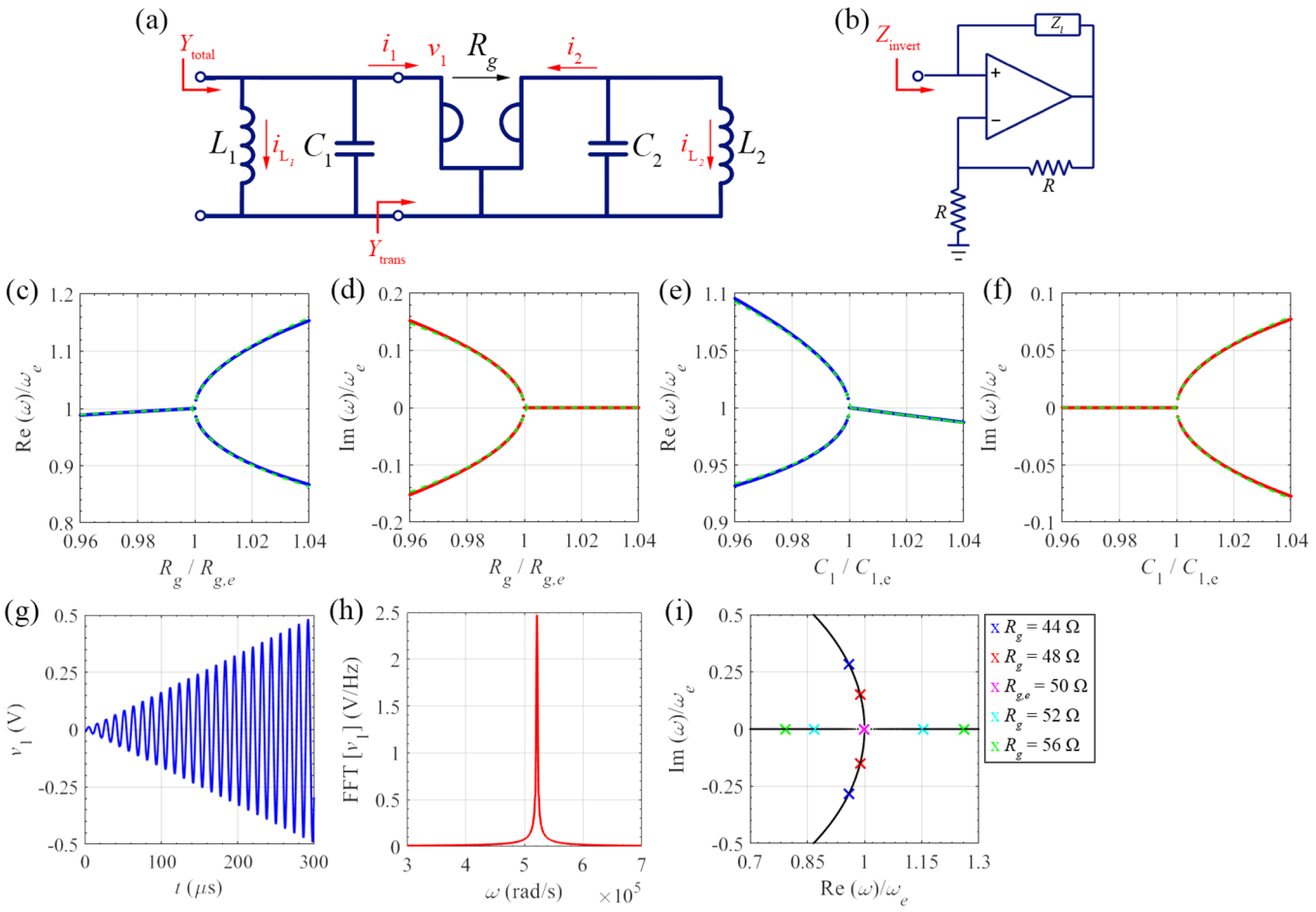

Fig. 2. (a) The gyrator-based circuit with the ideal gyrator connected two parallel LC tanks. (b) Opamp-based circuit configuration to obtain negative inductance and capacitance. The sensitivity of the (c), (e), real and (d), (f), imaginary parts of the eigenfrequencies to (c), (d) gyration resistance, (e), (f) positive capacitance C_1. Solid lines: solution of eigenvalue problem of equation (2); green-dashed lines: Puiseux series approximation truncated to its second term. Voltage of positive capacitance $v_1(t)$ at EPD (g) time-domain, and (h) frequency-domain. The frequency-domain result is calculated by applying an FFT with 10^6 samples in the time window of 0 to 3 ms. (i) Root locus of zeros of $Y_{total}(\omega) = 0$ showing the real versus imaginary parts of resonance frequencies by perturbing gyration resistance. At the EPD, two zero collide at ω_e and the system's total admittance has the form of $Y_{total}(\omega) \propto (\omega - \omega_e)^2$.

converts the impedance $Z_l(\omega)$ to $Z_{\text{invert}}(\omega) = -Z_l(\omega)$. Thus, we can provide the required negative capacitance and inductance by employing that configuration.

The real and imaginary parts of perturbed eigenfrequencies normalized to the EPD angular frequency by varying R_g are shown in Figures 2c and 2d, and analogous results by perturbing the positive capacitance C_1 are shown in Figures 2e and 2f. In addition, the eigenfrequencies are well approximated by using the Puiseux fractional power series expansion (green dashed lines). Appendix A provides the concept and formulas for this method. The approximated results obtained by the Puiseux series show an excellent agreement with the "exact" values calculated directly from the eigenvalue problem. The coefficients of the Puiseux series up to second-order for the mentioned example are calculated as, $\alpha_1 = 3.85 \times 10^5$ rad/s, and $\alpha_2 = 1.42 \times 10^5$ rad/s when perturbing R_g, and $\alpha_1 = j2.07 \times 10^5$ rad/s, and $\alpha_2 = -1.72 \times 10^5$ rad/s when perturbing C_1. The bifurcation of the real part of the eigenfrequencies, which indicate the stable sensing region, is observed when $R_g > R_{g,e}$, and $C_1 < C_{1,e}$.

Time-domain simulation result for the voltage $v_1(t)$ is obtained using the Keysight Advanced Design System (ADS) time-domain circuit simulator, and the result is plotted in Figure 2g. The frequency spectrum corresponding to the simulated time-domain voltage is found by taking the Fast Fourier Transform (FFT), as shown in Figure 2h. The results are obtained using the initial voltage of 1 mV on the left capacitor C_1. We observe that the voltage increases linearly with time. As well

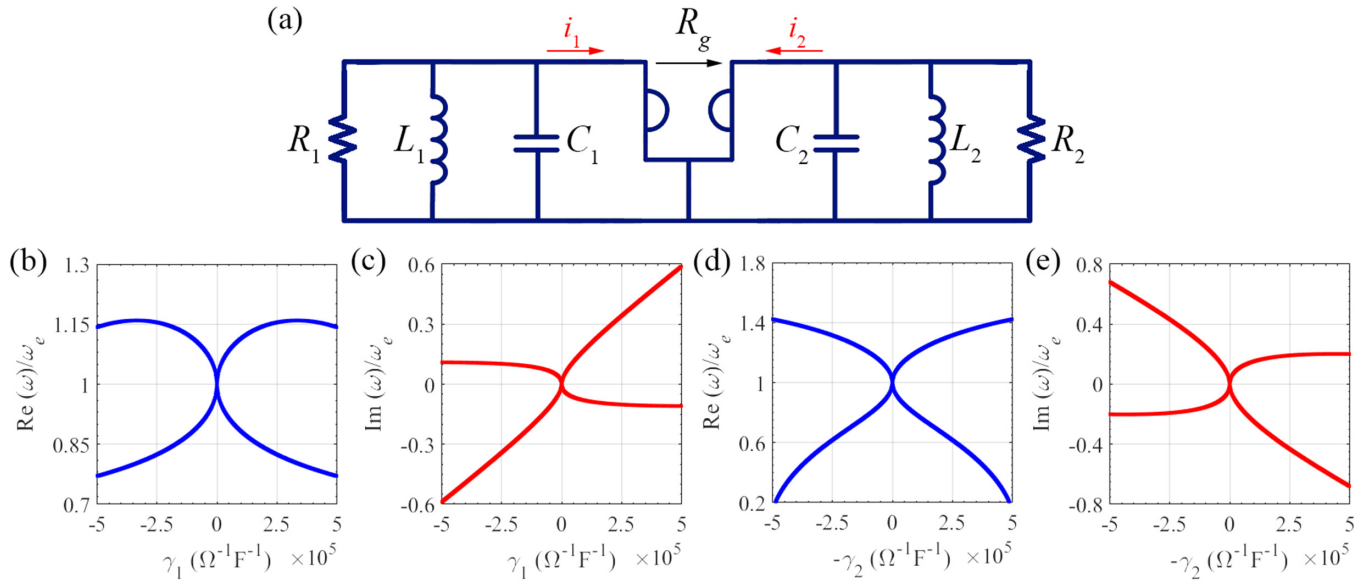

Fig. 3. (a) Schematic view of the lossy gyrator-based circuit, with a resistor in each resonator. Variation of (b) real and (c) imaginary parts of the angular eigenfrequencies to a resistor perturbation on the left resonator, i.e., when γ_1 changes and $\gamma_2 = 0$. Variation of (d) real and (e) imaginary parts of the angular eigenfrequencies to a resistor perturbation on the right resonator, i.e., when $-\gamma_2$ changes and $\gamma_1 = 0$.

known in circuit theory, this linear growth indicates that two system eigenvalues collided, and a double pole describes the system response. This is a specific property of a second-order EPD. The oscillation frequency is $\omega_o = 5.22 \times 10^5\,\mathrm{rad/s}$, which is exactly equal to EPD angular frequency ω_e.

We now observe the EPD in a frequency-domain analysis by calculating the circuit's total input admittance $Y_{total}(\omega)$, as shown in Figure 2a. We define the two admittances of two LC tanks as $Y_1 = j\omega C_1 + 1/(j\omega L_1)$ and $Y_2 = j\omega C_2 + 1/(j\omega L_2)$. Then the transferred admittance of the Y_2 to the left side is $Y_{trans}(\omega) = 1/\left(R_g^2 Y_2\right)$. The total admittance observed from the circuit input port is calculated by

$$Y_{total}(\omega) = Y_1(\omega) + Y_{trans}(\omega). \tag{9}$$

The resonant angular frequencies are achieved by imposing $Y_{total}(\omega) = 0$; the normalized resonance frequencies to the EPD angular frequency by varying the gyration resistance are shown in Figure 2i. Two zeros of total admittance coincide exactly at EPD.

3.2 Lossy configuration and stability

In this section, we study the loss effects on the eigenfrequencies of the gyrator-based circuit. Two parallel resistors R_1 and R_2 are connected to both resonators, as shown in Figure 3a. By writing down the circuit equations and assuming the same state vector as introduced in the lossless case, the associated Liouvillian formalism reads as

$$\frac{\mathrm{d}\boldsymbol{\Psi}}{\mathrm{d}t} = \underline{\mathbf{M}}\boldsymbol{\Psi}, \tag{10}$$

$$\underline{\mathbf{M}} = \begin{bmatrix} 0 & 0 & 1 & 0 \\ 0 & 0 & 0 & 1 \\ -\omega_{01}^2 & 0 & -\gamma_1 & \dfrac{1}{R_g C_2} \\ 0 & -\omega_{02}^2 & -\dfrac{1}{R_g C_1} & -\gamma_2 \end{bmatrix}, \tag{11}$$

where $\gamma_1 = 1/(R_1 C_1)$ and $\gamma_2 = 1/(R_2 C_2)$ represent the losses made by resistors. The eigenfrequencies are found by solving the characteristic equation,

$$\omega^4 - j\omega^3(\gamma_1 - \gamma_2) - \omega^2\left(\omega_{01}^2 + \omega_{02}^2 + \gamma_1\gamma_2 + \frac{1}{C_1 C_2 R_g^2}\right) + j\omega\left(\gamma_1\omega_{02}^2 + \gamma_2\omega_{01}^2\right) + \omega_{01}^2\omega_{02}^2 = 0. \tag{12}$$

Here, eigenfrequencies ω and $-\omega^*$ are both roots of the characteristic equation. In order to have a stable circuit, eigenfrequencies should be purely real, but the characteristic equation in equation (12) has some imaginary coefficients. Here, to have purely real eigenfrequencies in the lossy circuit, the odd-power terms of the angular eigenfrequency in the characteristic equation should vanish. Otherwise, a complex eigenfrequency is needed to satisfy the characteristic equation. There is no condition to make both ω and ω^3 coefficients equal to zero [23]. Hence, eigenfrequencies are always complex, leading to instabilities that cause oscillations in the circuit.

By considering the same value for components as already used in the lossless case, the evolution of eigenfrequencies is shown in Figures 3b and 3c. In these plots, loss on the first resonator is changed, and loss on the second resonator is eliminated. Moreover, in Figures 3d and 3e, we perturb the loss on the second resonator while the loss on the first resonator is removed. When both losses are

zero, the system has the same EPD frequency of a lossless configuration, but perturbed eigenfrequencies are complex-valued for any amount of losses. So, the lossy circuit oscillates at the frequency associated with the real part of the unstable eigenfrequency. Also, the eigenfrequency is extremely sensitive to either positive or negative variations in the parallel resistances (square root behavior due to the perturbation). A working option is based on preventing the circuit from reaching saturation by switching off the circuit and operating on the circuit's transient response, as was done in [25] for an EPD based on a time modulated circuit.

4 EPD in PT-symmetric coupled resonators and nonlinearity effects

This section discusses the EPD in two mutually coupled resonators based on PT-symmetry. This is the circuits studied so far by most of the researchers in the last decade [7,18–20,22]. We show the occurrence of an EPD by using the concept of the eigenvector coalescence parameter. Moreover, we study the resonance condition when the total admittance of the circuit is equal to zero (i.e., the double zero condition). The negative conductance in the analyzed circuit could be achieved via cross-coupled or opamp-based circuits. The negative conductance obtained from these transistor-based circuits has nonlinearity effects due to the saturation. Thus, the nonlinearity in negative conductance would alter the circuit operation, as discussed later on. We model the nonlinearity with a cubic i-v characteristic and show the time-domain analysis and frequency responses by using time-domain simulations that are the right tool when nonlinearity is present.

Moreover, we stress the EPD sensitivity characteristic and provide an example where the sensing scheme involves the perturbation of a capacitance. It means that the PT-symmetry is broken. We demonstrate the high sensitivity behavior of the eigenfrequencies for either positive or negative changes in capacitance and show that the system becomes unstable. In [18], the authors discussed sensitivity using two PT-symmetric coupled resonators. They demonstrated the sensitivity of the eigenfrequencies of the circuit due to the capacitance perturbation while they kept the PT-symmetry configuration. Thus, they needed to tune the other (nonsensing) side of the circuit to have balanced capacitance on both sides to keep the PT-symmetry even after each sensing operation. It means that the exact value of the changes in the sensing capacitance should be somehow known to tune the other side, which is not possible in practical sensing scenarios. Also, they could only measure the perturbation in the bifurcation direction (i.e., only the negative (or positive) capacitance changes, based on the design). Both positive and negative capacitance perturbation sensing ranges should be desirable, and the tuning process should be made easier since there is no priori knowledge of the sensing capacitance variation. Hence, it is not possible to keep the system PT-symmetric while sensing unless possible iterative schemes are researched that guess the unknown capacitance value. Finally, we confirm the eigenfrequency's sensitivity and square root behavior to the perturbation by using the Puiseux fractional power series expansion.

4.1 EPD in mutual coupled resonators with PT-symmetry

Two coupled LC tanks terminated on the left side with a gain given by the negative conductance $-G_1$ and terminated on the right side with loss G_2 are illustrated in Figure 4a. By writing Kirchhoff's current law, we obtain the two equations for the circuit

$$\begin{cases} \ddot{Q}_1 = -\dfrac{Q_1}{LC_1(1-k^2)} + \dfrac{kQ_2}{LC_2(1-k^2)} + \dfrac{G_1}{C_1}\dot{Q}_1 \\ \ddot{Q}_2 = \dfrac{kQ_1}{LC_1(1-k^2)} - \dfrac{Q_2}{LC_2(1-k^2)} - \dfrac{G_2}{C_2}\dot{Q}_2 \end{cases}, \quad (13)$$

where Q_1 is the capacitor charge on the gain side (left resonator), Q_2 is the capacitor charge on the loss side (right resonator), and $k = M/L$ is the transformer coupling coefficient. In addition, $\dot{Q}_1$, $\ddot{Q}_1$, $\dot{Q}_2$, and $\ddot{Q}_2$ are the first and the second time derivatives of the capacitors' charge. We define the state vector as $\boldsymbol{\Psi} \equiv \left[Q_1, Q_2, \dot{Q}_1, \dot{Q}_2\right]^{\mathrm{T}}$ where superscript T denotes the transpose operation. Therefore, the circuit evolution is described by

$$\frac{\mathrm{d}\boldsymbol{\Psi}}{\mathrm{d}t} = \underline{\mathbf{M}}\boldsymbol{\Psi}, \quad (14)$$

$$\underline{\mathbf{M}} = \begin{bmatrix} 0 & 0 & 1 & 0 \\ 0 & 0 & 0 & 1 \\ \dfrac{-1}{LC_1(1-k^2)} & \dfrac{k}{LC_2(1-k^2)} & \dfrac{G_1}{C_1} & 0 \\ \dfrac{k}{LC_1(1-k^2)} & \dfrac{-1}{LC_2(1-k^2)} & 0 & -\dfrac{G_2}{C_2} \end{bmatrix}. \quad (15)$$

Assuming signals in the form of $Q_n \propto e^{j\omega t}$, $C_1 = C_2 = C_0$ and $G_1 = G_2 = G$; we get the eigenfrequencies of the circuit by solving the characteristic equation, $\det(\underline{\mathbf{M}} - j\omega\underline{\mathbf{I}}) = 0$, leading to

$$\begin{cases} \omega_{1,3} = \pm\omega_0\sqrt{\dfrac{1}{1-k^2} - \dfrac{\gamma^2}{2} - \sqrt{b}} \\ \omega_{2,4} = \pm\omega_0\sqrt{\dfrac{1}{1-k^2} - \dfrac{\gamma^2}{2} + \sqrt{b}} \end{cases}, \quad (16)$$

where

$$b = -\frac{1}{1-k^2} + \left(\frac{\gamma^2}{2} - \frac{1}{1-k^2}\right)^2. \quad (17)$$

In the above equations, $\gamma = G\sqrt{L/C_0}$ and $\omega_0 = 1/\sqrt{LC_0}$. According to equation (17), the required condition to obtain an EPD is $b = 0$, which leads to an EPD

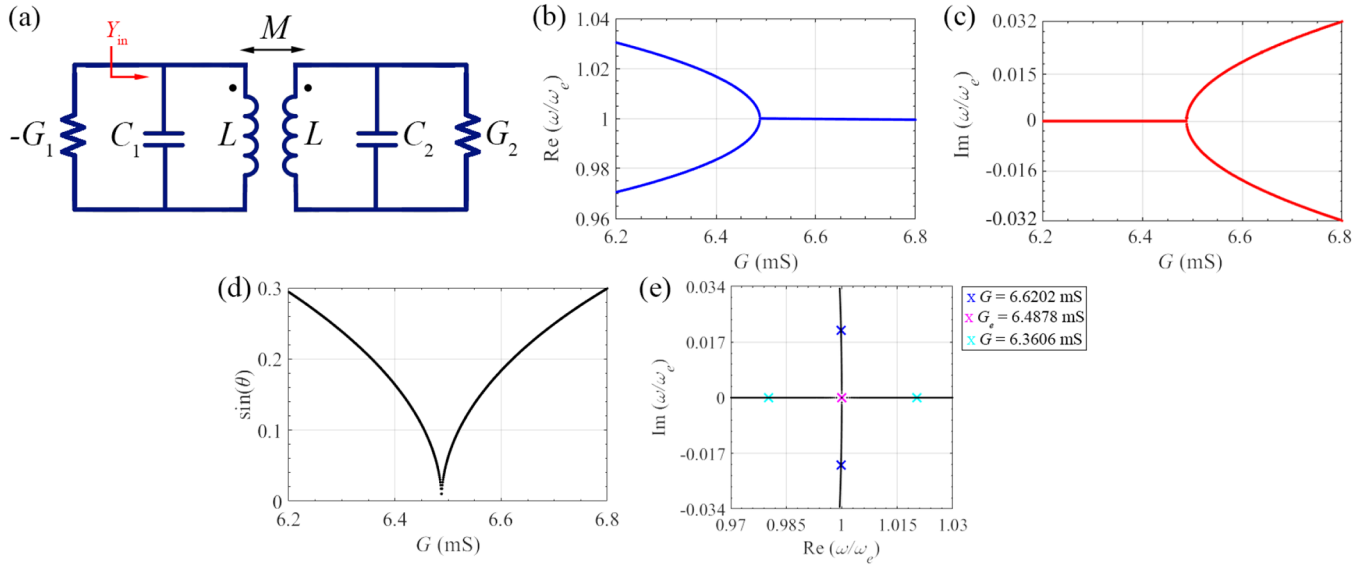

Fig. 4. (a) Two mutually coupled LC tanks terminated with balanced gain on the left and loss on the right side $G_1 = G_2 = G$; (b) real and (c) imaginary parts of evaluated eigenfrequencies by perturbing G. In the illustrated plots, only eigenvalues with the positive real parts are drawn. (d) The coalescence factor corresponding to calculated eigenvectors which showing the degeneracy of two eigenvectors exactly at G_e(e) Root locus of zeros of $Y_{in}(\omega) - G = 0$ showing the real and imaginary parts of resonance frequencies of the circuit when perturbing both load resistance and gain G. At the EPD, the system's total admittance is $Y_{in}(\omega) - G_e \propto (\omega - \omega_e)^2$; hence it shows a double zero at ω_e.

angular frequency of

$$\omega_e = \frac{\omega_0}{\sqrt[4]{1-k^2}}. \tag{18}$$

In the presented example, we use $L = 1\,\mu\text{H}$, $C_1 = C_2 = 1\,\text{nF}$, where inductors are mutually coupled via $k = 0.2$, and terminated with balanced gain and loss $G_1 = G_2 = G$. After solving the eigenvalue problem, the evolution of real and imaginary parts of the eigenfrequencies are shown in Figures 4b and 4c. The eigenfrequencies of the circuit coalesce at a specific balanced gain/loss value of $\gamma = \gamma_e = 0.205$, where γ_e that leads to an EPD is derived as

$$\gamma_e = \frac{1}{\sqrt{1-k}} - \frac{1}{\sqrt{1+k}}. \tag{19}$$

To validate the results, we assume $\gamma = 0$, which means there is no gain or loss in the system and it results in two simple mutual LC tanks. The mentioned circuit has two pairs of eigenfrequencies $\omega_{1,3} = \pm\omega_0/\sqrt{1+k}$ and $\omega_{2,4} = \pm\omega_0/\sqrt{1-k}$. If we remove the coupling, i.e., $k = 0$, the eigenfrequencies are equal to the independent LC tank circuits $\pm\omega_0$. For the values, $0 < \gamma < \gamma_e$, the system's eigenfrequencies are purely real, and the system has two fundamentals real eigenfrequencies. For the values, $\gamma_e < \gamma$, the two eigenfrequencies are complex conjugate, and system solutions grow or damp depending on the sign of the imaginary part of the angular eigenfrequencies; the system exhibits self (unstable) oscillations at the frequency associated with the real part of the eigenfrequency. The eigenvector coalescence factor is defined to evaluate how the circuit's operation point is close to an EPD and measure the coalescence of two eigenvectors. It is defined as $\text{C.F.} = |\sin(\theta)|$, where $\cos(\theta)$ is

$$\cos(\theta) = \left(\frac{|\langle \boldsymbol{\Psi}_1, \boldsymbol{\Psi}_2 \rangle|}{||\boldsymbol{\Psi}_1||\ ||\boldsymbol{\Psi}_2||}\right). \tag{20}$$

In the determined equation $\langle\ ,\ \rangle$ is the inner product and $\|\ \|$ denotes the eigenvector norm. The coalescence factor for the presented example is shown in Figure 4d. As we observe in this plot, two eigenvectors have coalesced at the corresponding value for EPD.

4.2 Root locus of zeros of admittance

In this section, the resonance condition based on the vanishing of the total admittance is studied. We find the admittance Y_{in}, shown in Figure 4a, and demonstrate its double zero at the EPD. The resonance condition for this circuit is expressed as

$$Y_{in}(\omega) - G = 0. \tag{21}$$

Here, the circuit is PT-symmetric, assuming linear gain and loss with $G_1 = G_2 = G$. We calculate the eigenfrequency by finding the zeros of the $Y_{in}(\omega) - G$, which results in the same eigenfrequencies obtained from $\det(\underline{\mathbf{M}} - j\omega\underline{\mathbf{I}}) = 0$. From the zeros trajectory, both ω and $-\omega$ and ω and ω^* are solutions of equation (21), and we only show the eigenfrequencies with positive real value in Figure 4e.

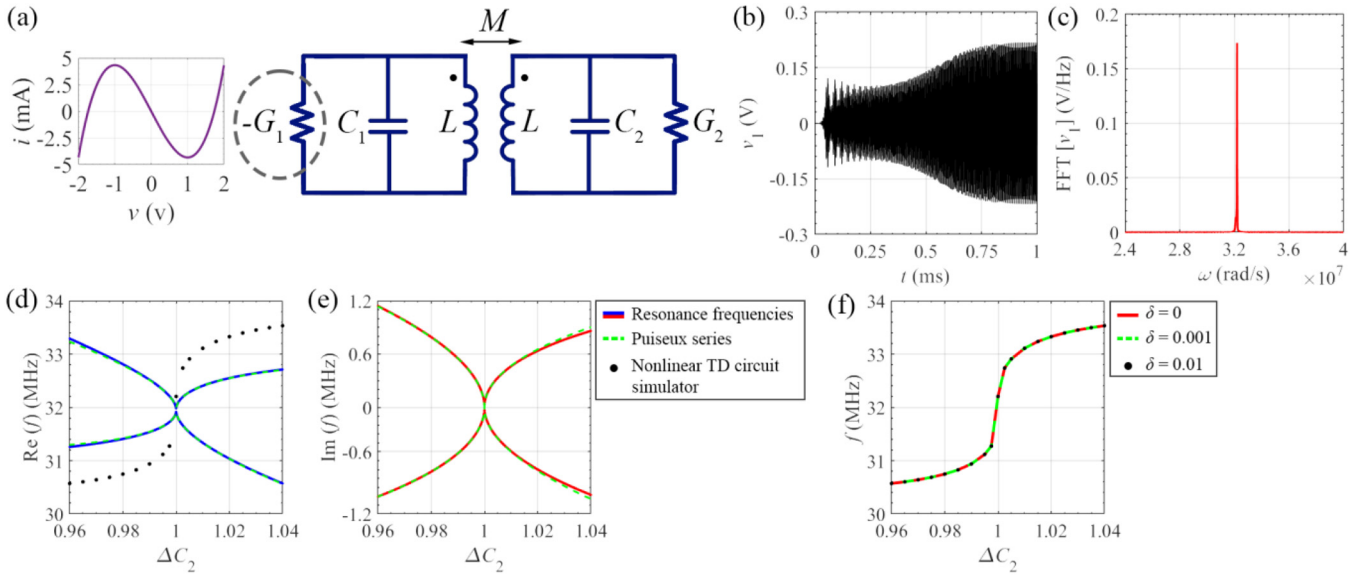

Fig. 5. (a) Two mutually coupled LC tanks terminated with nonlinear gain on the left and linear loss resistance on the right side where always $G_1 = 1.001 \times G_2$. (b) Time domain response. (c) Frequency response of the gain-side capacitor voltage at the EPD point. (d) Real and (e) imaginary parts of the eigenfrequencies versus load capacitance perturbation ΔC_2; solid line: result from $\det(\underline{\mathbf{M}} - j\omega\underline{\mathbf{I}}) = 0$; green dashed line: Puiseux fractional power series expansion terminated to its second order; black dots are obtained from the nonlinear time domain simulation. (f) Oscillation frequency versus load capacitance perturbation for three different mismatches between gain and loss $\delta = 0$, 0.001, 0.01: the three different gains provide the same saturated oscillation frequencies.

4.3 Nonlinear gain and oscillator characteristics

In this section, we discuss the oscillator characteristics and nonlinear gain effects in two wireless coupled resonators, as in Figure 5. The transient and frequency response of the system are discussed when using a cubic (nonlinear) negative conductance model of the gain element. The system's parameters are the same as in the previous section where $G_1 = G_2 = G_e = 6.49$ ms, and the EPD angular frequency is $\omega_e = 3.19 \times 10^6$ rad/s. The relation between voltage and current of the nonlinear negative conductance is [53]

$$i = -G_1 v + \alpha v^3, \tag{22}$$

where $-G_1$ is the small-signal negative conductance and $\alpha = G_1/3$ is a third-order nonlinearity that is related to the active device's saturation. We now assume the small-signal nonlinear gain G_1 to be slightly bigger than the balanced loss, as $G_1 = 1.001\, G_2 = 1.001\, G_e$ to make the circuit slightly unstable (slightly breaking PT-symmetry). The time-domain response and frequency response obtained from Keysight ADS time-domain circuit simulator are shown in Figures 5b and 5c, where the circuit operates in the proximity of the EPD. To show the sensitivity of this oscillator, we perturb the capacitor C_2 on the lossy side by 0.5%. The oscillation frequency at each perturbation, shown with the black dots, is found by taking the FFT of the time-domain voltage signal at the capacitor C_1 (on the gain side) after reaching saturation. The FFT is calculated by using 10^6 samples in the time window of 1000 periods after saturation, for each perturbed case. The system shows a distinct saturated oscillation frequency at each perturbed capacitor value. The frequency shift from the case without perturbation could be easily measured. For the sake of comparison with the linear case, solid blue and red lines in Figures 5d and 5e show the eigenfrequency evolution versus load capacitance perturbation as $\Delta C_2 = (C_2 - C_{2,e})/C_{2,e}$ ($C_{2,e}$ is the capacitor's value at EPD) by assuming linear gain for $-G_1$. The green dashed lines show the Puiseux fractional power series expansion truncated to its second order, which exhibits the square-root-like sensitivity of the eigenvalues to a perturbation. Using both linear and nonlinear gain, the resonance frequency behavior shows the square root variation with capacitance perturbation. The difference in the frequency values between the nonlinear time-domain simulation and theoretical eigenvalue solutions arises from the nonlinearity and the subsequent saturation regime. The Puiseux series coefficients are calculated as, $\alpha_1 = 5.35 \times 10^6 - j4.84 \times 10^6$ rad/s, and $\alpha_2 = -7.90 \times 10^6 - j1.62 \times 10^6$ rad/s.

The use of nonlinear gain in the circuit and the saturation effects make the EPD sensing regime robust. An error-correction method is discussed to enhance the robustness of sensing using nonlinearity in [54]. Also, the nonlinearity works as a self-correcting process in two coupled optical ring resonators in [55]. Nonlinearity in our proposed circuit helps maintain the oscillation frequency at the EPD frequency, within a range of small mismatches between gain and loss. The results obtained from the simulation shown in Figure 5f demonstrate that even with a 1% mismatch between gain and loss, the circuit oscillates at the same frequency as the case with balanced loss and gain.

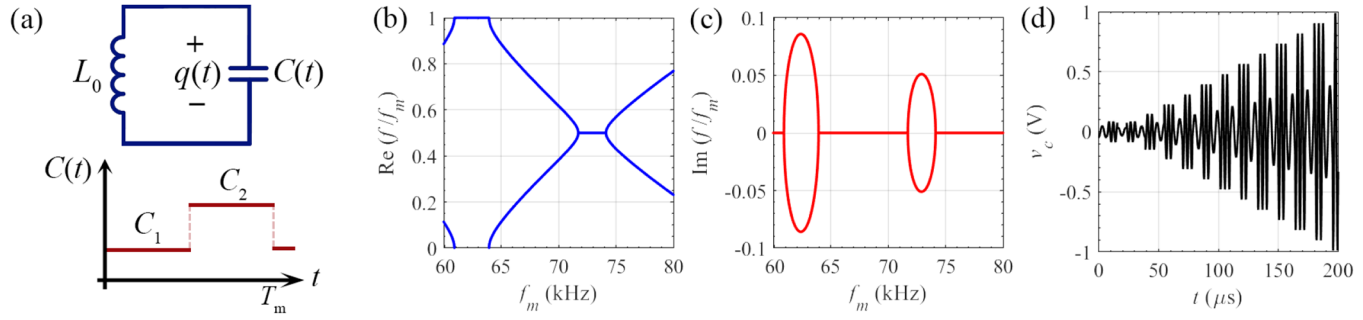

Fig. 6. (a) Time periodic capacitor connected to the inductor in parallel. The capacitor varies between two values C_1 and C_2 with T_m period, as shown as an inset. (b) Real and (c) imaginary parts of resonanse frequency evolution varying modulation frequency f_m. (b) The time domain signal revealing the second order EPD due to the capacitor's voltage linear growth, with initial condition of $v_c(0^-) = 50\,\text{mV}$, and $f_m = 63.95\,\text{kHz}$.

The red curve shows the oscillation frequency for the system with an exact match between the (nonlinear) small-signal gain and loss (i.e., $G_1 = G_2$), the dashed green is related to the case with $G_1 = 1.001\,G_2$, and the black points denote the case with even larger small-signal gain, $G_1 = 1.01\,G_2$. They all show the same results in terms of shifted oscillation frequency versus C_2 perturbation.

5 EPD in a time-varying single resonator

We now discuss a completely different way to obtain an EPD in a *single resonator* containing a time-varying element. It can be used as a highly sensitive circuit. As in the PT-symmetry system with balanced gain and loss discussed in the previous section, the EPD's highly sensitive characteristics are also found in the time-varying single resonator, without the need for a gain component. For instance, we show an EPD in a periodic time-varying simple LC circuit in Figure 6a. We summarize the general formulation that can be applied to electronic and optical circuits. By assuming the state vector $\boldsymbol{\Psi}(t) = [\Psi_1(t), \Psi_2(t)]^{\mathrm{T}}$ where T is the transpose operator. The differential equation describing the state vector time evolution is

$$\frac{\mathrm{d}\boldsymbol{\Psi}(t)}{\mathrm{d}t} = \underline{\mathbf{M}}(t)\boldsymbol{\Psi}(t), \tag{23}$$

where $\underline{\mathbf{M}}(t)$ is the 2×2 time-variant system matrix. Here, the system matrix changes periodically in time, unlike the cases discussed in Sections 3 and 4. Thus, we do not have only one system matrix, and we employ time-periodic analysis to achieve eigenvalues using the *transition matrix*. For LTV systems with period T_m, the state vector evolution from the time instant t to $t + T_m$ is given by

$$\boldsymbol{\Psi}(t + T_m) = \underline{\boldsymbol{\Phi}}(t + T_m, t)\boldsymbol{\Psi}(t), \tag{24}$$

where $\underline{\Phi}(t_2, t_1)$ is the state transition matrix that transfers the state vector $\boldsymbol{\Psi}$ from t_1 to t_2 [56]. The eigenvalue problem is

$$(\underline{\boldsymbol{\Phi}} - \lambda\,\underline{\mathbf{I}})\boldsymbol{\Psi}(t) = 0, \tag{25}$$

where $\underline{\mathbf{I}}$ is a two-by-two identity matrix and λ represents an eigenvalue. The eigenvalues are found by solving the characteristic equation $\det(\underline{\boldsymbol{\Phi}} - \lambda\,\underline{\mathbf{I}}) = 0$, leading to

$$\begin{cases} \lambda_p = \dfrac{\mathrm{tr}(\underline{\boldsymbol{\Phi}})}{2} \pm \sqrt{\left(\dfrac{\mathrm{tr}(\underline{\boldsymbol{\Phi}})}{2}\right)^2 - \det(\underline{\boldsymbol{\Phi}})}, p = 1, 2 \\ \boldsymbol{\Psi}_p(t) = \left[\Phi_{12}, \lambda_p - \Phi_{11}\right]^T \end{cases} \tag{26}$$

where Φ_{12} and Φ_{11} are elements of the two-by-two matrix $\underline{\boldsymbol{\Phi}}$. For the illustrated circuit in Figure 6a, the eigenvalues are $\lambda_p = e^{j2\pi f_p T_m}$, with $p = 1,\ 2$, where f_p are the two resonance frequencies, with all $f_p \pm nf_m$ harmonics (n is the integer number with modulation frequency $f_m = 1/T_m$).

We now demonstrate the degeneracy in an LTV−LC tank shown in Figure 6a. The capacitance $C(t)$ varies between two values $C_1 = 1.5\,C_0$ and $C_2 = 0.5\,C_0$ with period T_m, where $C_0 = 20\,\text{nF}$.

Defining the state vector $\boldsymbol{\Psi}(t) = [q(t),\ i(t)]^{\mathrm{T}}$ with capacitor's charge $q(t)$ and the inductance current $i(t)$, we find the system matrix as

$$\underline{\mathbf{M}}_p = \begin{bmatrix} 0 & -1 \\ 1/(L_0 C_p) & 0 \end{bmatrix},\ p = 1, 2. \tag{27}$$

The resonant frequencies versus modulation frequency f_m are shown in Figures 6b and 6c. We restrict the plot to frequencies with positive real value, in the range of $0 < f/f_m < 1$, which could be identified as the fundamental Brillouin Zone (BZ) in a time-varying system. EPD happens at $f_{m,e} = 71.72\,\text{kHz}$ and $f_{m,e} = 63.95\,\text{kHz}$, where the subscript e denotes the corresponding value at the EPD. At an EPD, two eigenvectors and eigenvalues collide, corresponding to a non-diagonalizable transition matrix $\underline{\boldsymbol{\Phi}}$ with a degenerate eigenvalue λ_e which is related to the resonance frequency f_e. In this configuration, two scenarios may happen to have the EPD (i.e., when the state transition matrix $\underline{\boldsymbol{\Phi}}$ is equivalent to a second-order Jordan-Block matrix). First, when the degenerate eigenvalue is $\lambda_e = -1$, which is related to a resonance frequency $f_e = f_m/2$, and due to the time periodicity, it also happens at harmonics ($f_e = f_m/2 \pm nf_m$). Second, when $\lambda_e = 1$, which is related to $f_e = 0$ and to the harmonics $f_e = \pm nf_m$. Note that here we assume a

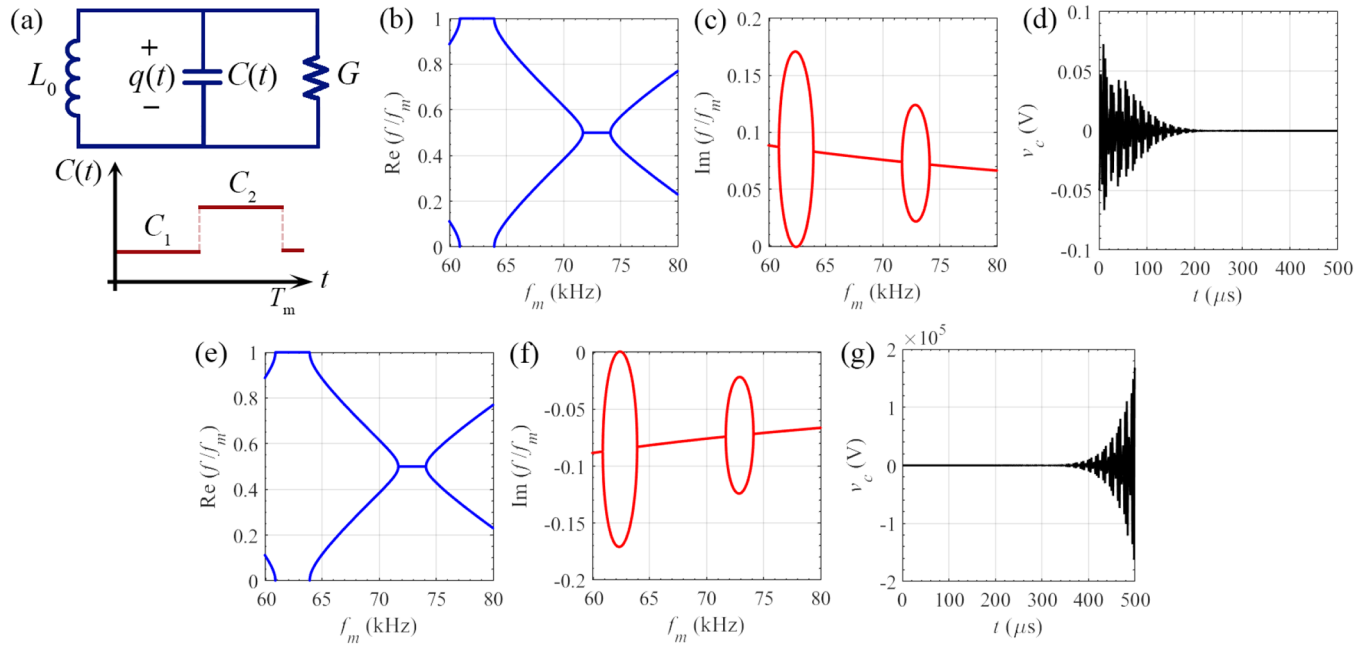

Fig. 7. (a) Time periodic capacitor $C(t)$ connected to the inductor L_0 and associated loss/gain G in parallel. The capacitor varies between two values C_1 and C_2 with T_m period, as shown in the subset. (b) Real and (c) imaginary parts of resonance frequency evolution varying modulation frequency f_m where the LC tank is connected to the lossy conductance $G = 1$ mS. (d) The time domain signal of the second order EPD which is indicated the decaying signal associated to the positive imaginary part of eigenfrequencies. (e) Real and (f) imaginary parts of resonance frequency evolution varying modulation frequency f_m where the LC tank is connected to the negative conductance $G = -1$ mS. (g) Capacitor's voltage obtained from Keysight ADS circuit simulator, which shows the rising signal. In all time domain simulation, the capacitor has an initial condition of $v_c(0^-) = 50$ mV.

lossless LC tank (besides the energy injection due to time variation), and we consider the loss effects later on. For modulation values such that $63.95\,\text{kHz} < f_m < 71.72\,\text{kHz}$, the system has two real resonance frequencies, whereas for modulation frequency such that $71.72\,\text{kHz} < f_m < 74.13$ kHz, the system experiences complex resonance frequencies, which cause instability and oscillation (rising signal associated with the resonance frequency's negative imaginary part). Here, we tend to work on the stable part, which has two different real resonance frequencies. At the EPD frequency associated with a modulation frequency of $f_m = 63.95$ kHz, the capacitor's voltage grows linearly, considering the initial condition of $v_c(0^-) = 50$ mV, which indicates that two eigenfrequencies have coalesced.

5.1 Loss effects on LTV circuit

We shall consider and study loss effects. To validate the occurrence of the EPDs in temporally LC resonator with losses, we assume an LC tank where the constant conductance G is associated to the losses or gain is connected in parallel, as shown in Figure 7a. In this circuit, the capacitance C changes between two-level capacitance ($C_1 = 1.5C_0$ and $C_2 = 0.5C_0$) with period T_m, as in the previous lossless case. We consider two scenarios where we connect the system to a loss ($G > 0$) or gain ($G < 0$) element. Defining the state vector $\boldsymbol{\Psi}(t) = [q(t),\ i(t)]^{\mathrm{T}}$ with capacitor's charge $q(t)$ and the inductance current $i(t)$, we find the system matrix as

$$\underline{\mathbf{M}}_p = \begin{bmatrix} -G/C_p & -1 \\ 1/(L_0 C_p) & 0 \end{bmatrix},\ p = 1, 2. \tag{28}$$

5.1.1 Time-varying capacitor: lossy case ($G > 0$)

The eigenfrequencies' dispersion diagram in Figures 7b and 7c show real and imaginary parts of the eigenfrequencies versus modulation frequency shown. The system parameters are the same as those as in the previous section: $L_0 = 33\,\mu$H, $C_0 = 20$ nF, $G = 1$ mS. Figure 7d shows the capacitor's voltage at the EPD associated with $f_m = 63.95$ kHz due to the initial condition of $v_c(0^-) = 50$ mV obtained from Keysight ADS time-domain circuit simulator. In this configuration, the LTV circuit with loss shows that the imaginary part of the eigenfrequency at every EPD is positive. The state vector, which contains the capacitor's voltage and inductor current, is proportional to the $e^{j\omega t}$. An eigenfrequency with a positive imaginary part leads to a decaying signal (exponential decay in system state vector), as shown for the case in Figure 7d.

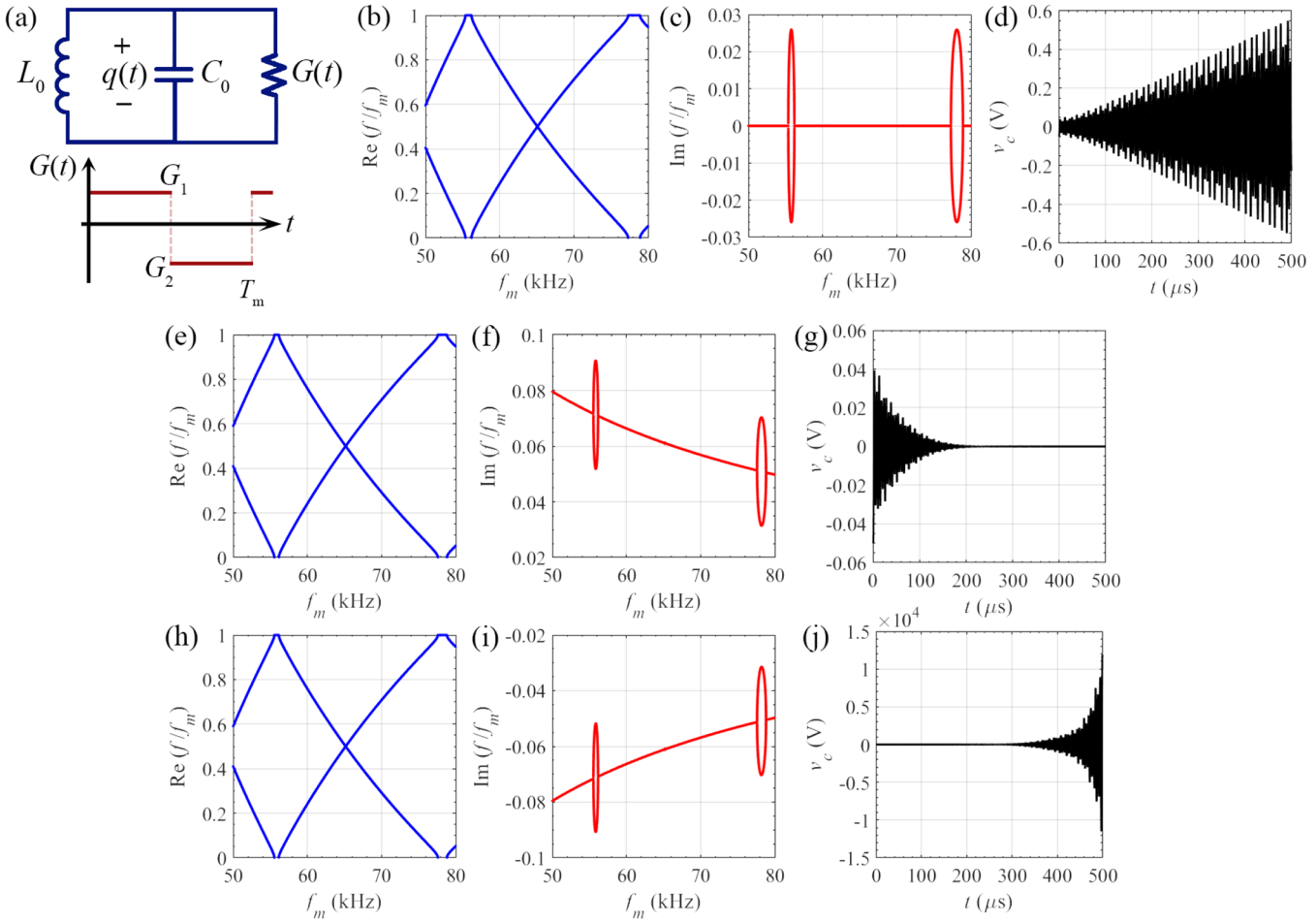

Fig. 8. (a) Circuit scheme including LC tank connected to the time-varying loss. (b) Real and (c) imaginary parts of eigenfrequency versus modulation frequency f_m, where the loss average is zero. (d) Time-domain signal capacitance's voltage $v_c(t)$, which shows the linear growth at EPD. (e) real and (f) imaginary parts of eigenfrequency versus modulation frequency f_m, where the loss average is positive (G works as a lossy component in average). (g) Time-domain signal capacitance voltage $v_c(t)$ is decaying related to the positive imaginary part of eigenfrequency at EPD. (h) Real and (i) imaginary parts of eigenfrequency versus modulation frequency f_m, where the loss average is negative (G works as a gain component in average). (j) Time-domain signal capacitance voltage $v_1(t)$ is rising related to the negative imaginary part of eigenfrequency at EPD. In all time-domain simulation the capacitor has an initial condition of $v_c(0^-) = 50\,\text{mV}$.

5.1.2 Time-varying capacitor: gain case ($G<0$)

Figures 7e and 7f show the real and imaginary parts of the system's eigenfrequencies where the system's parameters are selected as $L_0 = 33\,\mu\text{H}$, $C_0 = 20\,\text{nF}$, $G = -1\,\text{mS}$. The negative conductance G here shows the gain which results in EPD frequencies with a negative imaginary part. Thus, the state vector is rising exponentially and making the system unstable. Figure 7g shows the capacitor's voltage at an EPD associated to $f_m = 63.95\,\text{kHz}$ due to the initial condition of $v_c(0^-) = 50\,\text{mV}$ obtained from Keysight ADS circuit simulator. The signal shows a rising behavior, which makes the system unstable and oscillating.

5.2 Time-varying conductance

In this section, we consider the time-varying loss/gain element with the time periodicity of T_m in the LTV circuit in Figure 8a. We show the occurrence of EPDs. The parallel conductance is set to G_1 for half period, and to G_2 for the other half. Generally, G_1 and G_2 could be positive and negative values acting as loss or gain in this scheme. By defining the state vector $\boldsymbol{\Psi}(t) = [q(t),\ i(t)]^{\mathrm{T}}$ with capacitor's charge $q(t)$ and the inductance current $i(t)$, we find the system matrix as

$$\underline{\mathbf{M}}_p = \begin{bmatrix} -G_p/C_0 & -1 \\ 1/(L_0 C_0) & 0 \end{bmatrix}, p = 1, 2. \tag{29}$$

We have three scenarios where the time average of the conductance,

$$\text{Avg}(G) = G_1 \frac{T_m}{2} + G_2 \frac{T_m}{2}, \tag{30}$$

is positive (lossy), negative (gain), and zero. The average $\text{Avg}(G) > 0$ means that loss is dominant, whereas $\text{Avg}(G) < 0$ means that gain is dominant, and when

$\mathrm{Avg}\,(G)=0$ the system has balanced gain and loss. The solution for the system's state vector $\boldsymbol{\Psi}$ (contains the solution of the charge on the capacitor and current on the inductor) is proportional to the eigenfrequency as $\boldsymbol{\Psi} \propto e^{j\omega t}$. The signal at an EPD, i.e., when the system experiences the coalescence of the eigenvalues at a real ω_e, voltages and currents grow linearly as $te^{j\omega t}$. This is due to the double pole in the Laplace transform of a signal of a system at the EPD. Moreover, when the eigenfrequencies are complex, signals in the system (currents and voltages) experience exponential growth or decay. In this section, the value of components in the LC tank is set as $L_0=33\,\mu\mathrm{H}$ and $C_0=20\,\mathrm{nF}$.

5.2.1 Time-varying conductance: zero average $\mathrm{Avg}\,(G)=0$

Figures 8b and 8c show the complex dispersion diagram, eigenfrequencies versus frequency modulation, with a zero time-average conductance. The conductance for half a period $T_m/2$ is $G_1=4\,\mathrm{mS}$ while for the other $T_m/2$ is $G_2=-4\,\mathrm{mS}$. The EPDs eigenfrequencies are real-valued here, and the dispersion diagram looks the same as the dispersion diagram of the lossless system. To validate it, we calculate the determinant of the transition matrix as

$$\det(\underline{\boldsymbol{\Phi}}) = e^{-\left(G_1\frac{T_m}{2}+G_2\frac{T_m}{2}\right)/(2C_0)}. \tag{31}$$

Thus, for zero time-average conductance ($\mathrm{Avg}\,(G)=0$) we have $\det(\underline{\boldsymbol{\Phi}})=1$, which leads to $\lambda_e=\pm 1$. Thus, under the mentioned conditions, the system has a real-valued EPD frequency f_e. Figure 8d shows the time-domain signal obtained from Keysight ADS that indicates the second-order EPD behavior associated to $f_m=56.2\,\mathrm{kHz}$, which exhibits a linear growth of the capacitor's voltage as $v_c \propto t\cos(\omega t+\theta)$.

5.2.2 Time-varying conductance: positive average $\mathrm{Avg}\,(G)>0$

The real and imaginary parts of the eigenfrequencies for positive time average conductance ($\mathrm{Avg}\,(G)>0$) are shown in Figures 8e and 8f. The system's parameters are, $G_1=4\mathrm{mS}$ and $G_2=-2\mathrm{mS}$, hence the loss is dominant in the system. The EPDs are complex frequencies with a positive imaginary part, which is associated with a damping signal in the circuit, as exhibited in Figure 8g, where modulation frequency is $f_m=56.2\,\mathrm{kHz}$.

5.2.3 Time-varying conductance: negative average $\mathrm{Avg}\,(G)<0$

Figures 8h and 8i show the real and imaginary parts of the eigenfrequencies for negative time average conductance ($\mathrm{Avg}\,(G)<0$). The conductances are $G_1=2\,\mathrm{mS}$ and $G_2=-4\,\mathrm{mS}$, hence the gain is dominant in the system. The EPDs frequencies have a negative imaginary part corresponding to an exponential rise of the signal making the system unstable, as shown in Figure 8j, where modulation frequency is $f_m=56.2\,\mathrm{kHz}$.

6 Conclusion

We considered three different circuit configurations supporting an EPD of order two: gyrator-based, PT-symmetry based, and linear time-varying systems. All the configurations exhibit ultra-sensitive responses to perturbations, though their operational regimes differ. Each design has some advantages compared to the others. For example, in a gyrator-based circuit, the system has purely real perturbed eigenfrequencies when perturbing one component (e.g., a capacitor), while negative capacitance and inductance are needed to realize such a circuit, which require active components. Small losses or gains in this circuit cause instability. Though it seems to be a complication at first sight and may require working in the transient regime before reaching saturation, instability offers the possibility to work in the unstable oscillatory regime. An EPD is also present in two coupled resonators with balanced gain and loss, i.e., satisfying PT symmetry. The presence of gain in one side of the circuit requires active electronic components to provide a precise gain value. To achieve the sensitive feature of the EPD, a component is varied in a standard sensing scheme (e.g., a capacitor), and the perturbed resonant frequency is detected. However, the sensing scheme proposed in the PT-symmetry regime required tuning the capacitance on the nonsensing part of the circuit to keep the circuit under PT-symmetry while the sensing component is varied [18]. This was done to keep the two shifted frequencies real-valued and avoid instabilities. (However, in a sensing scheme, the value of the varied component is usually the one to be measured; hence it is not known a priori). This complication is not needed in the circuit using the gyrator, and it is also not needed in the circuit based on the single LTV resonator.

Compared to the conventional PT-symmetric circuit where people observed shifted resonance frequencies [18,20], here instead, we have shown that we can work in an oscillatory regime generated by the instability and the nonlinear behavior of the circuit. In other words, we have turned the instability due to broken PT-symmetry (due to a perturbation) to our advantage. The oscillation frequency after reaching saturation is very sensitive to perturbations. Still, it shows the square-root-like dependency with respect to perturbations and the possibility to measure both signs of an element perturbation (this is not possible with the other schemes in the linear regime discussed in this paper). This nonlinear oscillator scheme is also robust in terms of bringing the system near the EPD, independent of the amount of (nonlinear) small gain used.

Finally, EPDs are found in linear time-varying single resonator circuits where a time-varying capacitor is connected to an inductor. There is no need for gain and lossy elements, though the time modulation requires active components. The effect of additional loss and gain has been discussed for this circuit. We have also shown that time-varying gain or loss connected to a stationary LC tank is another method that leads to EPDs. The simple tuning procedure is one important advantage of the LTV circuit compared to gyrator-based and PT-symmetric circuits. In PT-symmetric and gyrator-based circuits, a tuning process

is needed to obtain an EPD, e.g., variable capacitors, gain, or resistors are deemed necessary. On the other hand, in the LTV circuit, the EPD is found by simply changing the modulation frequency, which is done easily in electronics. Note that to obtain the system's resonance frequency, we need a long enough time interval to measure the signal to derive its frequency response with good accuracy. Thus, the rise/fall time of the signal is important. In this paper, we used the practical quantities as modulation frequency discussed in [25]. There are two work regimes for the system to study the resonance frequencies evolution. First, the circuit needs to be reset periodically, like the circuit in [23], and resonance frequencies are found by looking at the transient response. Second, let the system saturate and then study the system in an oscillatory regime. Note that the system must be designed properly to have a rational rise/fall time in signals. At the same time, fast rising or damping signals cause losing the frequency response resolution.

This material is based upon work supported by the National Science Foundation (NSF) awards ECCS-1711975 and by the Air Force Office of Scientific Research Award No. FA9550-19-1-0103.

Appendix A: Puiseux fractional power series expansion

The sensitivity of a system due to the perturbation of a system's component is detected by measuring changes in the system's observables, like the system's resonance frequency. The Puiseux fractional power series expansion helps us find the eigenvalues ω_p related to the perturbations when working at an EPD of order p. We consider a small perturbation Δ_X of a system parameter X as

$$\Delta_X = \frac{X - X_e}{X_e}, \tag{A1}$$

where X_e is the parameters' value at the EPD, and X is the parameter's value after applying perturbation.

Away from an EPD of order p, the system matrix $\underline{\mathbf{M}}$ is diagonalizable, and there are p independent eigenvectors. Whereas at an EPD, $\underline{\mathbf{M}}$ is non-diagonalizable, and the system has only one eigenvector and $p-1$ generalized eigenvectors, and p repeated eigenvalues (i.e., eigenfrequencies). Therefore, the system matrix is similar to a matrix that contains a $p \times p$ dimension Jordan block.

For a system with the characteristic equation of $\det(\underline{\mathbf{M}}(\Delta_X) - j\omega\underline{\mathbf{I}}) = 0$, under the condition $\partial[\det(\underline{\mathbf{M}}(\Delta_X) - j\omega\underline{\mathbf{I}})]/\partial\omega \neq 0$ at the EPD, the $\underline{\mathbf{M}}$ matrix is made of a $p \times p$ Jordan block. Thus, the perturbed eigenfrequencies could be expressed by the Puiseux fractional power series expansion, including powers of $\Delta_X^{1/p}$ such as

$$\omega_p = \omega_e + \alpha_1\zeta + \alpha_2(\zeta)^2 + \alpha_3(\zeta)^3 + \ldots, \tag{A2}$$

where $\zeta = \exp(2\pi j/p)\Delta_X^{1/p}$ and the series is a kind of convergent Taylor series of power of $\Delta_X^{1/p}$. Note that the eigenvalues follow the Puiseux fractional power series expansion at and very near the EPD frequency is a way to validate the existence of an EPD (bifurcation of the eigenvalues). Equation (A2) shows that the eigenfrequency shift from an EPD $|\omega(\Delta_X) - \omega_e|$ is proportional to $\Delta_X^{1/p}$ for small Δ_X. For second order EPDs, a perturbation Δ_X results in the perturbed eigenvalues $\omega_p(\Delta_X)$ with $p = 1, 2$, and the Puiseux fractional power series expansion of $\omega_p(\Delta_X)$ is given by [3,57]

$$\omega_p(\Delta_X) \approx \omega_e + \alpha_1(-1)^p\sqrt{\Delta_X} + \alpha_2\Delta_X. \tag{A3}$$

The first two coefficients are expressed

$$\alpha_1 = \left(-\frac{\frac{\partial H(\Delta_X,\omega)}{\partial \Delta_X}}{\frac{1}{2!}\frac{\partial^2 H(\Delta_X,\omega)}{\partial \omega^2}}\right)^{\frac{1}{2}}, \tag{A4}$$

$$\alpha_2 = -\frac{\frac{\alpha_1^3}{3!}\frac{\partial^3 H(\Delta_X,\omega)}{\partial \omega^3} + \alpha_1\frac{\partial^2 H(\Delta_X,\omega)}{\partial\omega\partial\Delta_X}}{\alpha_1\left(\frac{\partial^2 H(\Delta_X,\omega)}{\partial\omega^2}\right)}, \tag{A5}$$

where $H(\Delta_X,\omega) = \det(\underline{\mathbf{M}}(\Delta_X) - j\omega\underline{\mathbf{I}})$. The coefficients are calculated at the EPD, i.e., at $\Delta_X = 0$ and $\omega = \omega_e$.

References

1. M.I. Vishik, L.A. Lyusternik, The solution of some perturbation problems for matrices and selfadjoint or non-selfadjoint differential equations I, Russian Math. Surv. **15**, 1 (1960)
2. P. Lancaster, On eigenvalues of matrices dependent on a parameter, Numerisc. Math. **6**, 377 (1964)
3. T. Kato, Perturbation Theory for Linear Operators (Springer-Verlag New York Inc., New York, 1966)
4. W.D. Heiss, A.L. Sannino, Avoided level crossing and exceptional points, J. Phys. A: Math. General **23**, 1167 (1990)
5. W.-H. Steeb, W.D. Heiss, Energy eigenvalue levels and singular point analysis, Phys. Lett. A **152**, 339 (1991)
6. A.P. Seyranian, Sensitivity analysis of multiple eigenvalues, J. Struct. Mech. **21**, 261 (1993)
7. C.M. Bender, S. Boettcher, Real spectra in non-Hermitian Hamiltonians having PT symmetry, Phys. Rev. Lett. **80**, 5243 (1998)
8. W.D. Heiss, Repulsion of resonance states and exceptional points, Phys. Rev. E **61**, 929 (2000)
9. C.M. Bender, M.V. Berry, A. Mandilara, Generalized PT symmetry and real spectra, J. Phys. A **35**, L467 (2002)
10. A. Figotin, I. Vitebskiy, Oblique frozen modes in periodic layered media, Phys. Rev. E **68**, 036609 (2003)

11. A. Figotin, I. Vitebskiy, Gigantic transmission band-edge resonance in periodic stacks of anisotropic layers, Phys. Rev. E **72**, 036619 (2005)
12. A. Guo et al., Observation of PT-symmetry breaking in complex optical potentials, Phys. Rev. Lett. **103**, 093902 (2009)
13. W.D. Heiss, The physics of exceptional points, J. Phys. A **45**, 444016 (2012)
14. B. Peng et al., Parity–time-symmetric whispering-gallery microcavities, Nat. Phys. **10**, 394 (2014)
15. F. Alex, V. Ilya, Slow light in photonic crystals, Waves Random Complex Media **16**, 293 (2006)
16. F. Alex, V. Ilya, Frozen light in photonic crystals with degenerate band edge, Phys. Rev. E. **74**, 066613 (2006)
17. M.V. Berry, Physics of nonhermitian degeneracies, Czechoslovak J. Phys. **54**, 1039 (2004)
18. P.-Y. Chen et al., Generalized parity–time symmetry condition for enhanced sensor telemetry, Nat. Electr. **1**, 297 (2018)
19. M. Sakhdari, M. Farhat, P.-Y. Chen, PT-symmetric metasurfaces: wave manipulation and sensing using singular points, New J. Phys. **19**, 065002 (2017)
20. J. Schindler, A. Li, M.C. Zheng, F.M. Ellis, T. Kottos, Experimental study of active LRC circuits with PT symmetries, Phys. Rev. A **84**, 040101 (2011)
21. H. Hodaei, M.-A. Miri, M. Heinrich, D.N. Christodoulides, M. Khajavikhan, Parity-time-symmetric microring lasers, Science **346**, 975 (2014)
22. T. Stehmann, W.D. Heiss, F.G. Scholtz, Observation of exceptional points in electronic circuits, J. Phys. A: Math. General **37**, 7813 (2004)
23. K. Rouhi, A. Nikzamir, A. Figotin, F. Capolino, Exceptional point in a degenerate system made of a gyrator and two unstable resonators, Phys. Rev. A **105**, 032214 (2022)
24. A. Nikzamir, K. Rouhi, A. Figotin, F. Capolino, Demonstration of exceptional points of degeneracy in gyrator-based circuit for high-sensitivity applications., arXiv preprint arXiv:2107.00639 (2021)
25. H. Kazemi, M.Y. Nada, A. Nikzamir, F. Maddaleno, F. Capolino, Experimental demonstration of exceptional points of degeneracy in linear time periodic systems and exceptional sensitivity, arXiv preprint arXiv:1908.08516 (2019)
26. H. Kazemi, M.Y. Nada, T. Mealy, A.F. Abdelshafy, F. Capolino, Exceptional points of degeneracy induced by linear time-periodic variation, Phys. Rev. Appl. **11**, 014007 (2019)
27. H. Kazemi et al., Ultra-sensitive radio frequency biosensor at an exceptional point of degeneracy induced by time modulation, IEEE Sensors J. **21** (2021)
28. A. Figotin, I. Vitebskiy, Oblique frozen modes in periodic layered media, Phys. Rev. E **68**, 036609 (2003)
29. M.Y. Nada, M.A.K. Othman, F. Capolino, Theory of coupled resonator optical waveguides exhibiting high-order exceptional points of degeneracy, Phys. Rev. B **96**, 184304 (2017)
30. A.F. Abdelshafy, T. Mealy, E. Hafezi, A. Nikzamir, F. Capolino, Exceptional degeneracy in a waveguide periodically loaded with discrete gain and radiation loss elements, Appl. Phys. Lett. **118**, 224102 (2021)
31. P.-J. Chen, S. Saati, R. Varma, M.S. Humayun, Y.-C. Tai, Wireless intraocular pressure sensing using microfabricated minimally invasive flexible-coiled LC sensor implant, J. Microelectromech. Syst. **19**, 721 (2010)
32. T.Q. Trung, S. Ramasundaram, B.-U. Hwang, N.-E. Lee, An all-elastomeric transparent and stretchable temperature sensor for body-attachable wearable electronics, Adv. Mater. **28**, 502 (2016)
33. Y. Feng, L. Xie, Q. Chen, L.-R. Zheng, Low-cost printed chipless RFID humidity sensor tag for intelligent packaging, IEEE Sensors J. **15**, 3201 (2015)
34. Y. Qian, N. Sahar, D. Prativa, N. Sangjun, H. Emily, K. Taeil, E. Rahim, All-3D-Printed, Flexible, and Hybrid Wearable Bioelectronic Tactile Sensors Using Biocompatible Nanocomposites for Health Monitoring, Adv. Mater. Technol. **7**, 2101034 (2021)
35. K. Rouhi, R. Marosi, T. Mealy, A.F. Abdelshafy, A. Figotin, F. Capolino, Exceptional degeneracies in traveling wave tubes with dispersive slow-wave structure including space-charge effect, Appl. Phys. Lett. **118**, 263506 (2021)
36. P.-J. Chen, D.C. Rodger, S. Saati, M.S. Humayun, Y.-C. Tai, Microfabricated implantable parylene-based wireless passive intraocular pressure sensors, J. Microelectromech. Syst. **17**, 1342 (2008)
37. S.R. Corrie, J.W. Coffey, J. Islam, K.A. Markey, M.A.F. Kendall, Blood, sweat, and tears: developing clinically relevant protein biosensors for integrated body fluid analysis, The Analyst **140**, 4350 (2015)
38. P. Tseng, B. Napier, L. Garbarini, D.L. Kaplan, F.G. Omenetto, Functional, RF-trilayer sensors for tooth-mounted, wireless monitoring of the oral cavity and food consumption, Adv. Mater. **30**, 1703257 (2018)
39. Y.J. Zhang et al., Noninvasive glucose sensor based on parity-time symmetry, Phys. Rev. Appl. **11**, 044049 (2019)
40. Z.-P. Liu et al., Metrology with PT-symmetric cavities: enhanced sensitivity near the PT-phase transition, Phys. Rev. Lett. **117**, 110802 (2016)
41. J. Wiersig, Enhancing the sensitivity of frequency and energy splitting detection by using exceptional points: application to microcavity sensors for single-particle detection, Phys. Rev. Lett. **112**, 203901 (2014)
42. J. Wiersig, Sensors operating at exceptional points: general theory, Phys. Rev. A **93**, 033809 (2016)
43. M.-A. Miri, A. Alù, Exceptional points in optics and photonics, Science **363**, 6422 (2019)
44. C.E. Rüter, K.G. Makris, R. El-Ganainy, D.N. Christodoulides, M. Segev, D. Kip, Observation of parity-time symmetry in optics, Nat. Phys. **6**, 192 (2010)
45. L. Feng, Z.J. Wong, R.-M. Ma, Y. Wang, X. Zhang, Single-mode laser by parity-time symmetry breaking, Science **346**, 972 (2014)
46. A. Figotin, Perturbations of circuit evolution matrices with Jordan blocks, J. Math. Phys. **62**, 042703 (2021)
47. A. Figotin, Synthesis of lossless electric circuits based on prescribed Jordan forms, J. Math. Phys. **61**, 122703 (2020)
48. B.D.H. Tellegen, The gyrator, a new electric network element, Philips Res. Rep. **3**, 81 (1948)
49. A. Antoniou, Gyrators using operational amplifiers, Electr. Lett. **3**, 350 (1967)

50. M. Ehsani, I. Husain, M.O. Bilgic, Power converters as natural gyrators, IEEE Trans. Circ. Syst I **40**, 946 (1993)
51. W.H. Holmes, S. Gruetzmann, W.E. Heinlein, High-performance direct-coupled gyrators, Electr. Lett. **3**, 45 (1967)
52. A. Nikzamir, K. Rouhi, A. Figotin, F. Capolino, Exceptional points of degeneracy in gyrator-based coupled resonator circuit, in 2021 Fifteenth International Congress on Artificial Materials for Novel Wave Phenomena (Metamaterials) (2021), pp. 302–304
53. D. Oshmarin, A.F. Abdelshafy, A. Nikzamir, M.M. Green, F. Capolino, Experimental demonstration of a new oscillator concept based on degenerate band edge in microstrip circuit, arXiv preprint arXiv:2109.07002 (2021)
54. S. Kananian, G. Alexopoulos, A.S.Y. Poon, Coupling-independent real-time wireless resistive sensing through nonlinear PT symmetry, Phys. Rev. Appl. **14**, 064072 (2020)
55. S. Ramezanpour, A. Bogdanov, Tuning exceptional points with Kerr nonlinearity, Phys. Rev. A **103**, 043510 (2021)
56. J.A. Richards, Analysis of Periodically Time-Varying Systems (Springer, Berlin Heidelberg, 1983)
57. A. Welters, On explicit recursive formulas in the spectral perturbation analysis of a Jordan block, SIAM J. Matrix Anal. Appl. **32**, 1 (2011)

Cite this article as: Alireza Nikzamir, Kasra Rouhi, Alexander Figotin, Filippo Capolino, How to achieve exceptional points in coupled resonators using a gyrator or PT-symmetry, and in a time-modulated single resonator: high sensitivity to perturbations, EPJ Appl. Metamat. **9**, 14 (2022)